Available online at www.sciencedirect.com

ScienceDirect

journal homepage: www.elsevier.com/locate/he

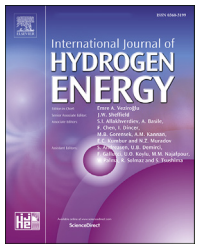

Preparing a novel gradient porous metal fiber sintered felt with better manufacturability for hydrogen production via methanol steam reforming

Jing-Rong Li [a], *Chang-Lin Yu* [a], *Zhi-Jia Xu* [a,*], *Qing-Hui Wang* [a], *Wei Zhou* [b], *Tian-Qing Zheng* [b]

[a] *School of Mechanical & Automotive Engineering, South China University of Technology, Guangzhou, 510640, China*
[b] *Department of Mechanical & Electrical Engineering, Xiamen University, Xiamen, 361005, China*

HIGHLIGHTS

- A novel gradient PCFSF is proposed as catalyst support for methanol SR.
- The PCFSF has simplified gradient porosity interfaces and better manufacturability.
- The reaction characteristics of the PCFSF are investigated by MSR experiments.
- The resultant performance is close to, even better than that of the non-simplified.

ARTICLE INFO

Article history:
Received 10 May 2019
Received in revised form
9 July 2019
Accepted 17 July 2019
Available online 7 August 2019

Keywords:
Methanol steam reforming
Porous metal fiber sintered felt
Gradient porosity configuration
Flow velocity distribution

ABSTRACT

The porous copper fiber sintered felts with gradient porosity structure (gradient PCFSFs) as catalyst supports is beneficial for heat and mass transfer for methanol steam reforming (MSR). However, the previously developed gradient PCFSF based on the velocity distribution introduces curved interface between different porosity portions, making the mold pressing method for its preparation more sensitive to tiny process changes. To improve its manufacturability, a novel gradient PCFSF with planar interface (PCFSF-SLR) is proposed in this paper by fabrication with multi-step mold pressing and solid phase sintering method using cutting copper fibers. Furthermore, MSR experiments under different gas hourly space velocities and reaction temperatures are conducted to verify the characteristics of PCFSF-SLR loaded with Cu/Zn/Al/Zr catalyst. The results have shown that the reaction characteristics of the PCFSF-SLR were similar to those with curved interfaces, and PCFSF-SLRs with a middle portion porosity of 0.9 have better hydrogen production performance and lower carbon monoxide concentration. More importantly, the results indicated that the methanol conversion and hydrogen flow rate of the gradient PCFSF with planar interface and porosity of 0.7-0.9-0.8 were close or even almost the same with that of the best gradient PCFSFs with curved interface and porosities of 0.7-0.9-0.8 and 0.8-0.9-0.7. Therefore, the proposed PCFSF-SLR provides a superior alternative to gradient PCFSFs with better manufacturability.

* *Corresponding author*. Room 403, 30# Building, Wushan Road 381#, Guangzhou, 510640, China.
E-mail addresses: lijr@scut.edu.cn (J.-R. Li), meycl@mail.scut.edu.cn (C.-L. Yu), mexzj@scut.edu.cn (Z.-J. Xu), wqh@scut.edu.cn (Q.-H. Wang), weizhou@xmu.edu.cn (W. Zhou), mszh@mail.xmu.edu.cn (T.-Q. Zheng).
https://doi.org/10.1016/j.ijhydene.2019.07.142

Introduction

Fuel cell is an energy-generating device without mechanical transmission component that can directly convert chemical energy of the fuel to electrical energy. The wide application prospect of the fuel cell is shown because of the advantages of high power generating efficiency and low noise [1–6]. Among them, polymer electrolyte membrane fuel cells (PEMFCs) have attracted a great attention on academic field due to the property of high energy density, rapid start up, and light-weight fuel processor [7–9]. In particular, pollutant zero-emission can be achieved with hydrogen fuel, which has high heat value and makes it possible for PEMFCs to work at lower temperatures. But in order to apply PEMFCs for portable devices, hydrogen supply is still a huge hurdle to overcome. Inflammable and explosive, coupled with low gas and liquid density, the storage and transportation of hydrogen is limited in consideration of security [10]. The use of renewable alcohols for catalytic reforming to achieve on-line hydrogen production is a good solution [11–13]. Among them, catalytic methanol steam reforming (MSR) is considered as one of the most effective solutions which has advantages of high stability, compact size and the ability of hydrogen supplying for fuel cells on board [14,15]. In addition, as a hydrogen-rich fuel, methanol is convenient for storage and transport.

In MSR reactors for hydrogen production, the catalyst support is a critical component, whose performance can greatly affect the activity, selectivity, and lifetime of the catalyst and the performance of the whole catalytic MSR system. Consequently, in order to obtain a higher MSR reaction efficiency, the catalyst support is required to have strong catalyst loading capacity and good performance of mass and heat transfer. Based on these requirements, many innovative catalytic MSR reactors have been continually emerging, and can be categorized into packed-bed and micro-structured according to the construction of the catalyst support. Generally, the latter is more applicable to transportation and portable power applications for the advantages of compact structure, relatively high electrical and thermal conductivities, when compared with packed-bed reactors [16]. Up to date, a variety of micro-structured reactors has been developed [17–19], with their performance being continuously optimized. Accordingly, novel catalyst supports with the characteristics of large specific surface area and lower pressure drop have been prepared to improve the reaction performance of micro-structured reactors for hydrogen production [17–19], including monolith [20,21], novel microchannel [22–25], foam metal [26,27], metal fibers [28–30], etc. Among them, monolithic microreactor, comprising a plurality of pore pipes inside, has the characteristics of small pressure drop and low cost. The catalyst is loaded on the surface of the pipe, thus causing problems such as low adhesion and easily shedding. The calcination of the catalyst material together with the microreactor material into the monolithic microreactor can effectively solve the above problems, but the method greatly limits catalyst material [18]. Microchannel reactor further reduces the volume of the microreactor by laser etching a series of channels on the metal sheet, but also increases the processing cost accordingly [22–25]. The foam metal prepared by the metal foaming process introduces interconnected pore structures, so that the volume utilization of the microreactor is greatly improved [26,27]. However, the preparation process has strict requirements on the raw materials and the processing parameters.

Different from the other catalyst supports, porous copper fiber sintered felts (PCFSFs) [28], manufactured by cutting method and solid sintered process, demonstrate properties that are highly expected for MSR hydrogen production. For instance, previous studies indicated that PCFSFs had larger superficial roughness (Ra is 5–20 μm, Ry 15–60 μm [31]) due to the simpler and lower-cost manufacturing process [28], which leads to higher specific surface area and stronger adhesion strength of catalyst. In addition, it was found that PCFSFs exhibited excellent mechanical properties, relatively high electrical and thermal conductivities. More importantly, inspired by the gradient strategy developed for other porous material preparation [32–38], PCFSFs with gradient porosities (Fig. 1(a)) had been recently prepared, and better performance of MSR hydrogen production was observed [39]. To further improve the performance of the gradient PCFSFs, an approach was proposed in our previous work [40] to partition the PCFSFs into sub-regions according to the best uniform velocity distributions of the reactant flow (Fig. 1(b)), determining the shape and position of the interfaces between sub-regions more reasonably. The experimental results showed that the MSR reaction performance of the novel gradient PCFSFs shown in Fig. 1(b) was generally better than that with planar interfaces presented in Fig. 1(a). In addition, the methanol conversion and the hydrogen flow rate of the novel gradient PCFSFs with porosity distribution along the Left-Right direction (PCFSF-LRs) is better than that with porosity distribution along the Upside-Underside direction (PCFSF-UUs). Thanks to the introduction of two additional design variables besides the porosity distribution, i.e. the shape and position of the interface between sub-regions, more freedom was provided for the design of PCFSF.

Nonetheless, despite the merits presented by the design method of PCFSF based on velocity distribution, it was found that the manufacturability of the method was weakened to some extent due to the curved interfaces between sub-regions. As it will be described in Subsection Simplification of the curved interfaces in PCFSF-LRs, the novel gradient PCFSF is firstly fabricated by a multi-step mold pressing process before being sintered. In this process, baffle plates with the same shape and size of the sub-regions of PCFSFs are utilized to pack and compress the copper fibers filled in the sub-regions one by one. However, in the previous study [40] it was found that if the interfaces between sub-regions were curved, it would be more difficult to fill the sub-regions with uniformly distributed copper fibers, especially near the curved interfaces. More specifically, sparser distribution of copper fibers near the curved interfaces was prone to appear. Consequently, the quality of the novel gradient PCFSF was more sensitive to tiny changes in the multi-step mold pressing process, whose repeatability required more time and experience, thus further lowering the efficiency.

To improve the manufacturability of the velocity distribution-based gradient PCFSF, and at the same time maintain the performance of hydrogen production as high as

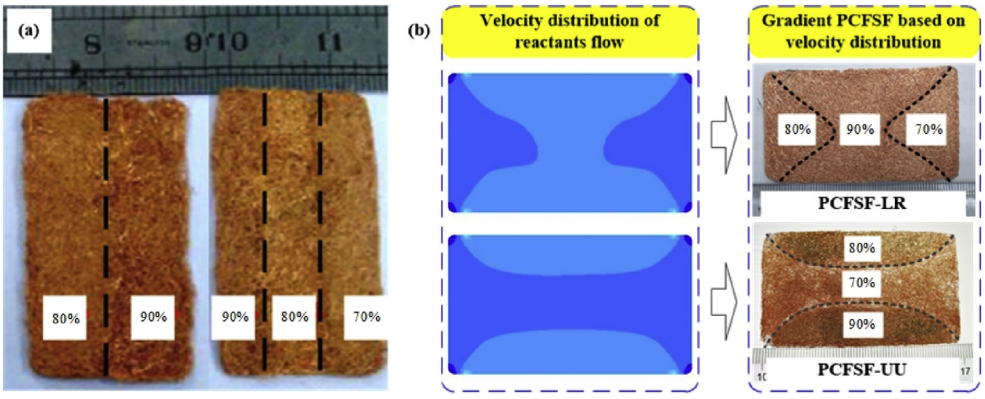

Fig. 1 – PCFSFs with gradient porosities (the percentage in the picture represents porosity). (a) Gradient PCFSFs with simple planar interfaces between sub-regions; (b) Gradient PCFSFs with curved interfaces between sub-regions based on velocity distribution of reactants flow [40].

possible, a method is proposed in this paper to simplify the curved interfaces between sub-regions. In this way, a method for gradient PCFSF preparation is preliminarily developed by simultaneously considering the flow velocity distribution and manufacturability. As is mentioned above, PCFSF-LRs exhibited better reaction performance than PCFSF-UUs did. Consequently, the simplification is based on PCFSF-LRs. After the preparation is accomplished, the fabricated gradient PCFSFs with simplified sub-region interfaces will be loaded with catalyst to investigate the MSR reaction performance of hydrogen production.

Methods

Simplification of the curved interfaces in PCFSF-LRs

In the previous study [40], one of the qualitative criteria was proposed to prepare PCFSFs with curved sub-region interfaces based on velocity distribution. Namely, the sub-regions of the velocity distribution should have areas close to each other, so that the partitioned sub-regions of PCFSFs would be large enough to have effective influence on the MSR reaction performance for hydrogen production. Following this criterion, the simplification of the curved interfaces in PCFSF-LRs is quite straightforward. The velocity distribution (see Fig. 1(b) and Fig. 2(a)) used to prepare PCFSF-LRs is simplified as the one presented in Fig. 2(b). Namely, the curved interfaces of PCFSF-LRs are simplified as planar ones, making a PCFSF be partitioned into three sub-regions with the same areas. For conciseness' sake, the simplified PCFSF-LRs are termed as PCFSF-SLRs in the following content of this paper.

Fabrication of the simplified PCFSF-SLRs

The manufacturing process of PCFSF-SLRs consists of three steps: including, in sequence, the fabrication of cutting fibers, the multi-step mold pressing process and the solid phase sintering process. Firstly, the continuous copper fibers were fabricated by cutting method on a common horizontal lathe (No: C6132A) with a multi-tooth cutting tool [28]. Thanks to the multi-tooth cutting tool, several tiny teeth can be involved in the cutting process simultaneously, so that the continuous copper fibers can be manufactured efficiently. The diameter of the cutting fiber was approximately 100 μm [19]. Then, the continuous copper fibers were chipped into short fiber segments with a length in the range of 10–20 mm to create beneficial condition for subsequent multi-step mold pressing.

In the second step, the packing chamber of the mold pressing equipment was partitioned into several portions through the baffle plates (Fig. 3). The nominal dimension of the packing chamber is $70 \times 40 \times 2\ mm^3$, the same with that of the reforming chamber will be shown in Fig. 5. With one of the baffle plate removed, the short copper fibers with random direction were uniformly put into the packing chamber of the mold pressing equipment, and then pressure was applied by screwing the bolts. After that, another baffle plate in the chamber portion was removed, and the copper fibers were then put into the chamber portion again. In this way, after all the partitioned chamber portions were filled with copper fibers, the mold pressing equipment was assembled with screws and nuts to ensure that the shot copper fibers were completely bonded to the packing chamber. The whole procedure of the multi-step mold pressing is shown in Fig. 3 and more details on assembly could be found in work [40]. It was noteworthy that for the same mold pressing process, the time (~10 min) used to prepare the PCFSF-SLRs was less than a half of the time (>20 min) to prepare PCFSF-LRs.

During the mold pressing process, the average porosity (E) of a sub-region in the PCFSF-SLRs is controlled according to the Volume-Quality method as shown in Eq. (1):

$$E(\%) = \left(1 - \frac{M}{\rho V}\right) \times 100 \quad (1)$$

where, V was the volume of a porosity portion of a PCFSF (cm^3), M was the mass of the portion (g) and ρ was the density of red copper (g/cm^3).

In the third step, the assembled mold pressing equipment filled with copper fibers was sintered using the solid-phase sintering method in the box-type furnace (NO.: FXL-12-11), which provided the hydrogen gas atmosphere with constant pressure of 0.3 MPa. The sintering temperature and holding

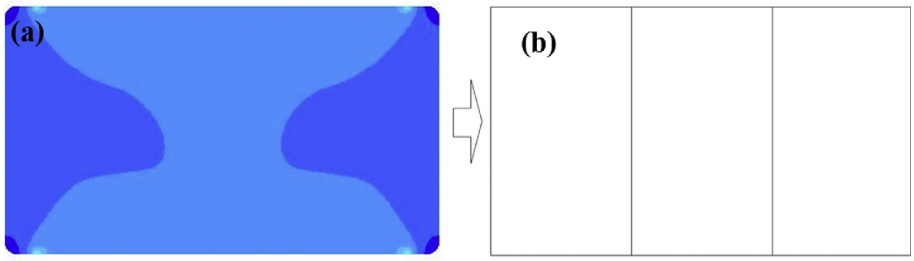

Fig. 2 – Simplification of PCFSF-LRs. (a) Velocity distribution with curved interfaces; (b) Simplified planar interfaces.

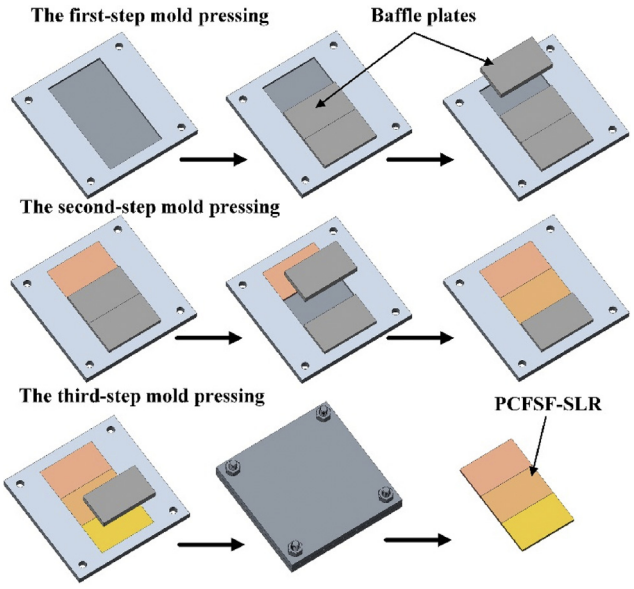

Fig. 3 – Schematic of the multi-step mold pressing process for PCFSF-SLRs preparation.

time were 900 °C and 30 min, respectively [39]. After the sintering was completed, the assembled mold pressing equipment in the furnace was cooled to room temperature. The remaining processes after the sintering process was the same as that in [40], thus will not be expanded.

Based on the above steps, a group of PCFSF-SLRs was prepared as shown in Fig. 4. To demonstrate the structures of the PCFSF-SLRs more clearly, the inlet and outlet area on the PCFSF-SLRs were also illustrated.

Loading catalyst and assembling laminated-sheet micro-reactor for performance test

Before loading catalyst, the PCFSF-SLRs were cleaned with ethanol in an ultrasonic bath for 5 min to remove any organic substance. The same Cu/Zn/Al/Zr catalyst (as well as the same loading method to perform the catalyst coating for PCFSF-SLRs) [28,39–42] developed more than 10 years ago was used in this paper, since the only difference between the PCFSF-SLRs and the previously developed gradient PCFSFs [39,40] is the configuration of the interfaces between different porosity portions. The co-precipitation method [27] was used to prepare the catalyst: the mixed solution of $Cu(NO_3)_2$, $Zn(NO_3)_2$, $Al(NO_3)_3$ and $Zr(NO_3)_4$, in the molar ratio of 11:6:4:1, was prepared in distilled water with the concentration of copper ion as 4.6%, and was further mixed with Al_2O_3 colloidal solution to obtain the catalyst precursor. Although Cu-based catalysts are the most common for MSR and reported to be more active and selective and less expensive than the group 8–10 metal-based catalysts [43], they suffer from the problems of pyrophoric characteristics and easy deactivation by thermal sintering at temperatures higher than 300 °C [44]. As a result, Al and Zr are usually added into the Cu-based catalysts as stabilizers or structural promoters [43]. The former was to strengthen the adhesion intensity of the catalyst on the surface of the copper fiber [28], while the latter could enhance the deoxidization of the copper and increase the surface area and the decomposition capability [45]. Thanks to the promoters, the temperatures for MSR based on Cu-based catalysts were reported as high as ~400 °C [46]. During the catalyst loading, wash-coating and wet impregnation methods were employed [27]. Namely, the PCFSF-SLRs were fully impregnated in the catalyst precursor solution, and then dried in an oven. The procedure was repeated until the catalyst loaded on each piece of PCFSF-SLRs (~9.96 g/each piece) reached about 0.50 g/9.96 g. The details of the Cu/Zn/Al/Zr catalysts and the preparation and loading method could be referred to [42]. After the catalyst loading, the PCFSF-SLR of 0.7-0.9-0.8 was used for vibration test (1–5 min) based on an ultrasonic device (No: KQ5200DB, Kunshan ultrasonic instruments Co., LTD, China) with an input power of 200 W. Results showed that the effective catalyst loading decreased from 0.455 g to 0.436 g, implying the good adhesion strength.

The PCFSF-SLRs loaded with catalyst was then embedded into the reforming chamber of the MSR micro-reactor (Fig. 5). Before the MSR reaction performance test, the catalyst needs to be pretreated and activated. Consequently, the PCFSF-SLRs loaded with catalyst were calcined at 400 °C for 2 h under N_2 flow rate of 100 ml/min. Then, it was calcined at 300 °C for 1 h in the mixture of N_2 (100 ml/min) and H_2 (50 ml/min).

Performance test of the MSR micro-reactor for hydrogen production

After assembling the MSR micro-reactor and activating the catalyst, methanol and distilled water in the molar ratio of 1:1.3 were premixed and fed into the vaporizing chamber to be gasified [42]. The gasified reactants were then transported into the reforming chamber to perform the MSR reaction, which includes three main reactions [41]:

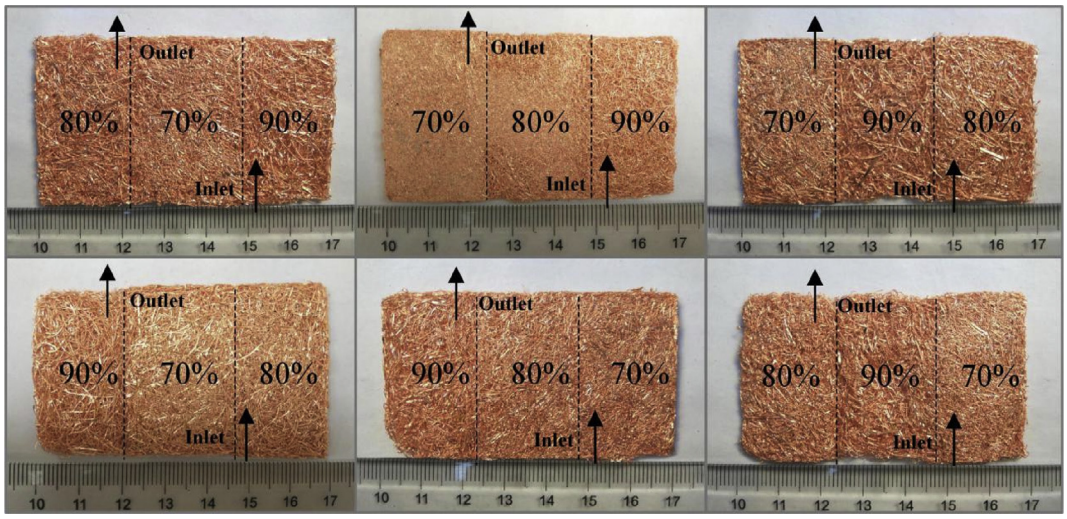

Fig. 4 – Appearance of PCFSF-SLRs with different porosity configurations.

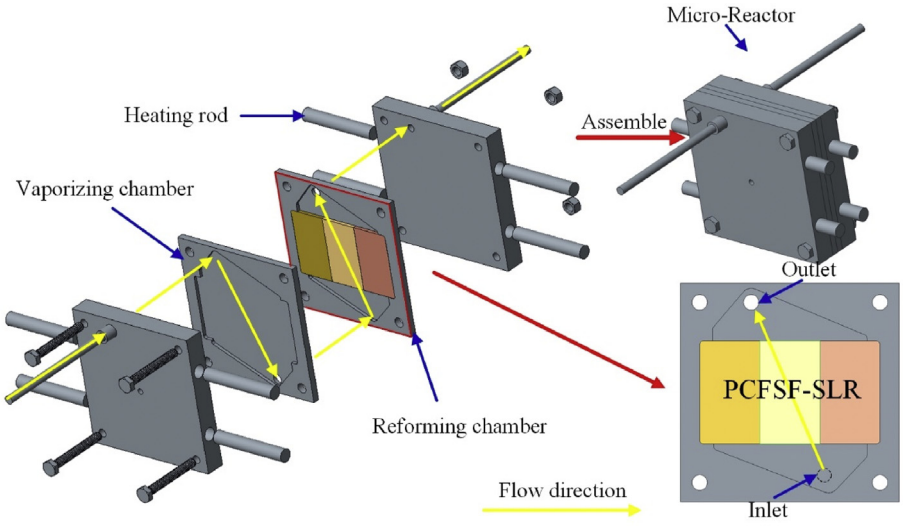

Fig. 5 – Schematic of the laminated-sheet micro-reactor with a PCFSF-SLR as catalyst support.

$$CH_3OH + H_2O \rightarrow CO_2 + 3H_2,\ \Delta H^{\circ}_{298} = +49.4\ kJ/mol \quad (2)$$

$$CH_3OH \rightarrow CO + 2H_2,\ \Delta H^{\circ}_{298} = +92.0\ kJ/mol \quad (3)$$

$$CO + H_2O \rightarrow CO_2 + H_2,\ \Delta H^{\circ}_{298} = -41.1\ kJ/mol \quad (4)$$

where Eq. (2), Eq. (3) and Eq. (4) are the total MSR reaction, the methanol decomposition reaction, and the water-gas shift reaction (WGS), respectively. The products of the reaction are hydrogen, carbon dioxide, a small amount of carbon monoxide, and unreacted methanol and water vapor. Part of the methanol and water vapor condensed in the pipeline made the measurement of the two components inaccurate, and the residual methanol and water vapor may introduce errors into the experimental results. As a result, the residual reactants were condensed and dried by a condenser pipe and a dryer to minimize the introduced errors. By doing so, the remained mixture of the reformatted gas detected included hydrogen, carbon dioxide and a small amount of carbon monoxide. The composition of the mixed gas was analyzed with an on-line gas chromatograph (NO.: GC-1690) equipped with a TCD detector. And the flow rate of the mixed gas was measured by a soap-bubble flowmeter.

Based on the analyzed data, three indicators were introduced to assess the MSR reaction performance for hydrogen production. The methanol conversion η was calculated according to C balance (Eq. (5)), and H_2 selectivity S_{H_2} was calculated by moles formed per mole methanol reacted (Eq. (6)); in addition, hydrogen flow rate v_{H_2} was calculated through Eq. (7).

$$\eta = \frac{y_{CO} + y_{CO_2}}{y_{CH_3OH}} \times 100\% \quad (5)$$

$$S_{H_2} = \frac{\frac{1}{3} \times y_{H_2}}{\left(y_{CO} + y_{CO_2}\right)} \times 100\% \quad (6)$$

$$v_{H_2} = F \times y_{H_2} \quad (7)$$

where y_{CO},y_{CO_2},y_{CH_3OH} and y_{H_2} were the volumetric fraction of carbon monoxide, carbon dioxide, methanol and hydrogen, respectively, and F was the normal flow rate of effluent gas.

During the performance test, the MSR reaction was conducted in the temperature range of 280–380 °C. The gas hourly space velocity (GHSV) of the mixture of methanol and distilled water fed for reaction was varied from 9,751.4 ml/(g·h) to 22,753.3 ml/(g·h). In order to reduce the error of the measured data, the gas velocity of the mixed gas was measured in each case for 10 times and an average value was taken.

Results and discussion

Methanol conversion and hydrogen flow rate

The methanol conversion and hydrogen flow rate for the PCFSF-SLRs under different reaction temperatures and GHSVs are shown in Fig. 6. In Fig. 6(a) and (b), the GHSV was fixed as 16,252.4 ml/gh. It could be found that the PCFSF-SLR of 0.7-0.9-0.8 had the best performance and could maintain methanol conversion over 90% and hydrogen flow rate above 0.45 mol/h from 300 °C to 380 °C. Besides, the methanol conversion and hydrogen flow rate of all PCFSF-SLRs slightly increased when temperature rose from 280 °C to 380 °C. Since MSR (Eq. (2)) was an endothermic reaction, high reaction temperature could increase the catalytic activity and accelerated the reaction rate, therefore causing the rise of hydrogen flow rate. This might also be the reason why the trend of the methanol conversion and the hydrogen flow rate with temperature was similar.

From Fig. 6(a) and (b), it could be further found that the methanol conversion and hydrogen flow rate of the PCFSF-SLRs were at a relatively low level when the reaction temperature was 280 °C, especially for PCFSF-SLRs of 0.7-0.8-0.9 and 0.9-0.8-0.7. The reason was that low reaction temperature would result into insufficient supply of heat energy, thus limiting the activation of catalysts for hydrogen production. Furthermore, the methanol conversion and hydrogen flow rate of the PCFSF-SLRs of 0.7-0.9-0.8, 0.8-0.9-0.7 and 0.7-0.8-0.9 were slightly decreased when the temperature exceeded 340 °C. However, no obvious trend was observed in other PCFSF-SLRs. This was attributed to two reasons. First, high temperature would inhibit the reaction of the exothermic reaction WGS (Eq. (4)), thus increasing the concentration of CO (Fig. 8(b)) and limiting the yield of hydrogen [47]. Second, when the temperature continuously rose, the flow rate of the reaction gas increased. Shorter residence time of the reactants led to a decrease in reaction efficiency, so as the decrease in methanol conversion. In addition, since the input rate of the reactant was fixed for a given GHSV, the decrease in methanol conversion would also cause the decrease of hydrogen flow rate.

Fig. 6(c) and (d) demonstrated methanol conversion and hydrogen flow rate of PCFSF-SLRs under different GHSVs (9,751.4 ml/(g·h) to 22,753.3 ml/(g·h)) and a fixed reaction

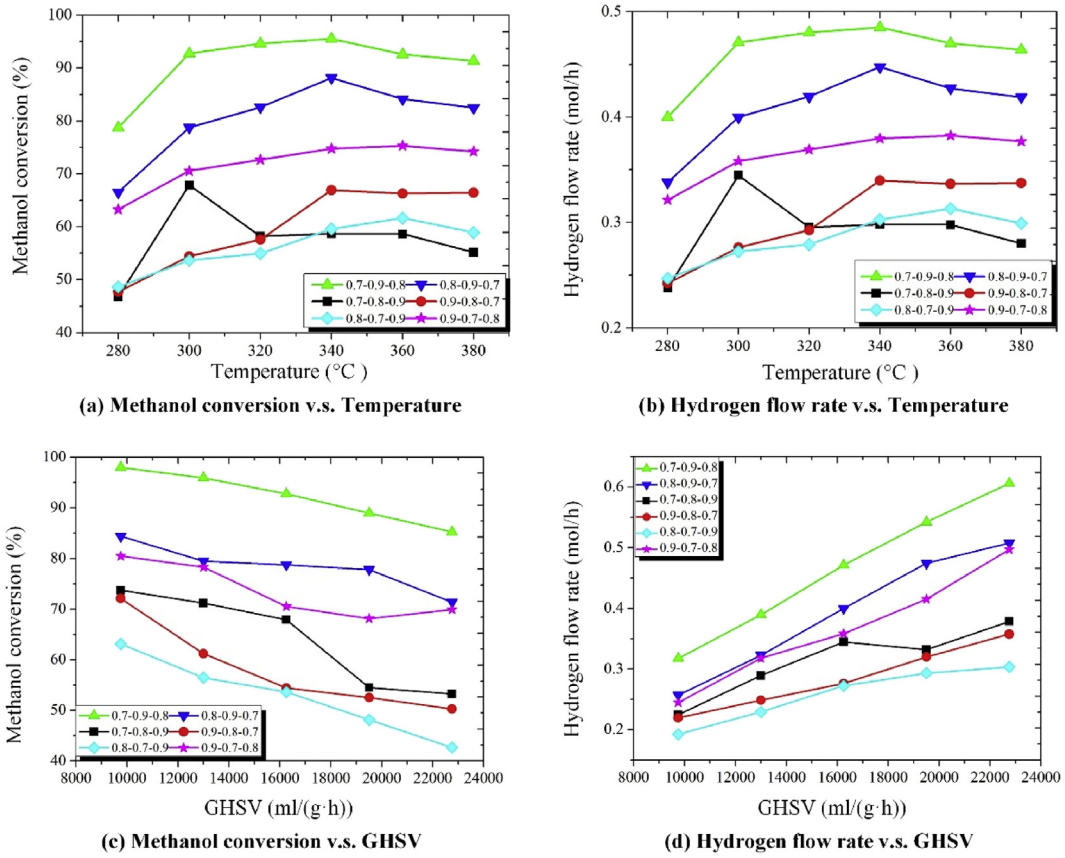

Fig. 6 – Methanol conversion and hydrogen flow rate for PCFSF-SLRs under different reaction temperatures and GHSVs.

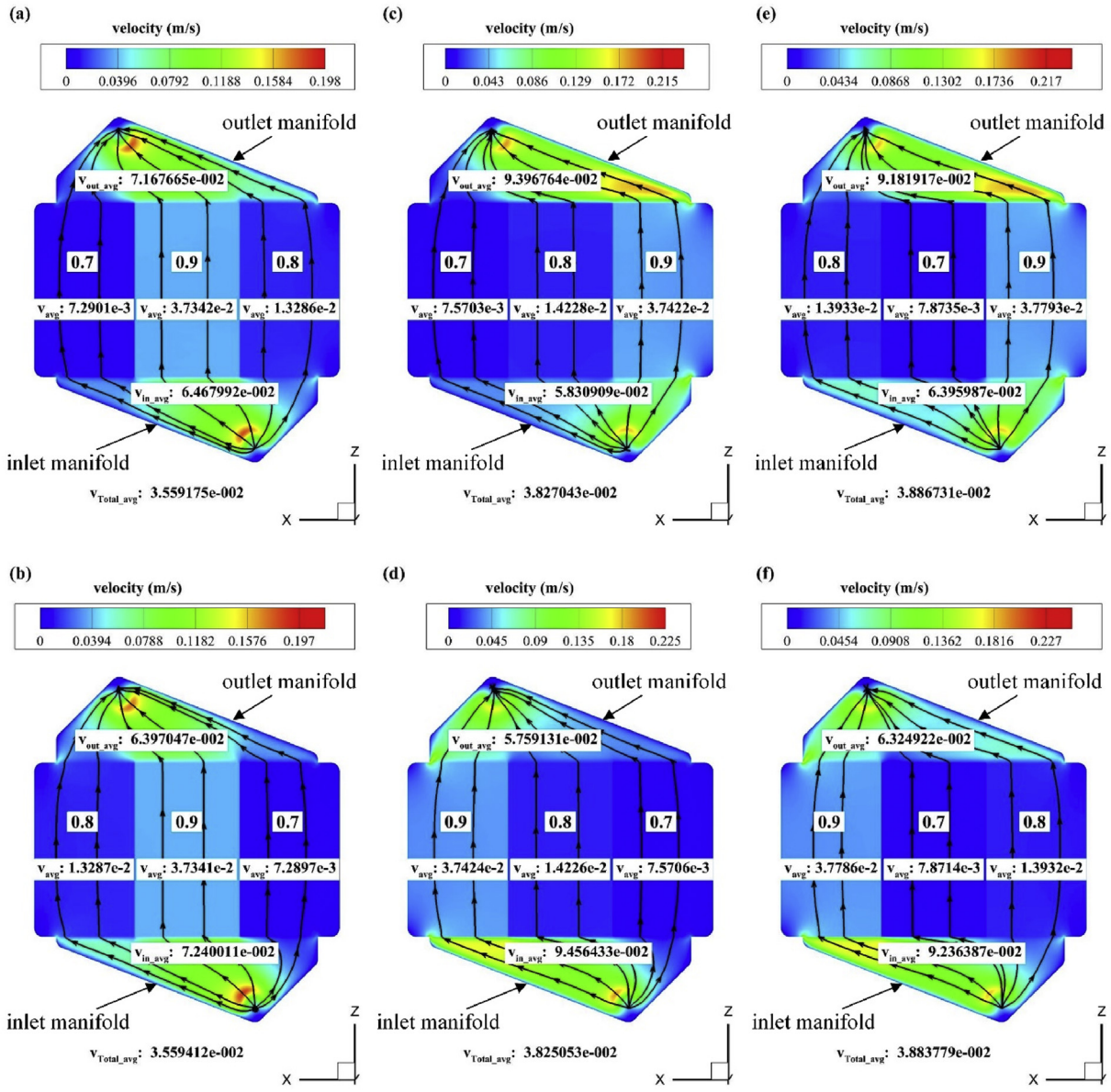

Fig. 7 – Flow velocity distributions of PCFSF-SLRs and inlet/outlet manifolds. v_{avg}, v_{in_avg}, and v_{out_avg} were the average velocity magnitude in the corresponding porosity sub-region of PCFSF-SLR, the inlet and outlet of the reaction chamber, respectively; and v_{Total_avg} was the average velocity magnitude of the whole reaction chamber.

temperature (300 °C), respectively. The methanol conversion could reach 98% at 9,751.4 ml/(g·h) for PCFSF-SLR of 0.7-0.9-0.8, and for which the hydrogen flow rate could reach 0.60 mol/h at 22,753.3 ml/(g·h). Obviously, it could be seen that methanol conversion decreased with the increase of GHSV, while hydrogen flow rate increased. Generally, the increase of GHSV could increase the total amount of reactants and the hydrogen generated. However, larger GHSV would not only increase the overall gas flow rate in the reforming chamber, but also reduce the residence time of the reactants, thus reducing the contact time between the reactants and the catalyst and making the methanol conversion decrease [39].

From Fig. 6, it was also easy to find that the PCFSF-SLRs differed greatly in methanol conversion and hydrogen flow rate. For example, it could be observed from Fig. 6 that the methanol conversion and hydrogen flow rate of PCFSF-SLRs of 0.7-0.9-0.8 and 0.8-0.9-0.7 were relatively higher. Especially, the methanol conversion and hydrogen flow rate of the PCFSF-SLR of 0.7-0.9-0.8 was higher than those of PCFSF-SLR of 0.8-0.9-0.7. Furthermore, the methanol conversion and hydrogen flow rate of the PCFSF-SLR of 0.8-0.7-0.9 were kept at a relatively low level. Obviously, porosity configurations of the PCFSF-SLRs would affect the overall hydrogen production performance greatly.

It had been recognized that flow velocity distribution in catalyst support is a fatal factor affecting the performance of micro-reactors for hydrogen production, and that more uniform flow velocity distribution will result into better hydrogen production performance [23,48–53]. As a result, to explain the performance difference of different PCFSF-SLRs, their flow

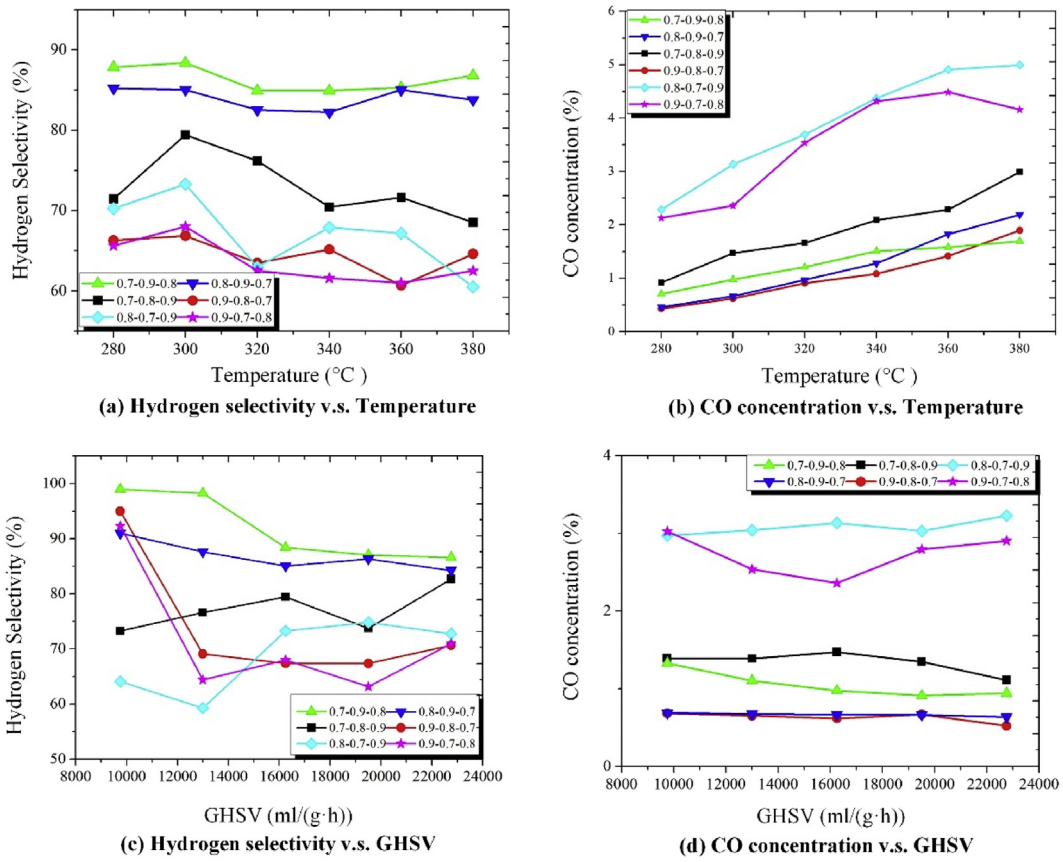

Fig. 8 – Hydrogen selectivity and CO concentration of PCFSF-SLRs under different reaction temperatures and GHSVs.

velocity distributions were analyzed as shown in Fig. 7, and from which several interesting phenomena were observed. First, the flow velocity distribution of each portion was different but relatively uniform. Second, when the porosity of the middle portion of the PCFSF-SLRs changed from 0.9 to 0.7, the average velocity magnitude in portions with the same porosity increased. For example, from Fig. 7(a), (c) and (e), it could be found that for PCFSF-SLRs of 0.7-0.9-0.8, 0.7-0.8-0.9 and 0.8-0.7-0.9 the average velocity magnitude in the portion with porosity of 0.7 increased with the decrease of middle portion porosity. This trend was also true for the average velocity magnitude of a whole PCFSF-SLR. Lower average velocity means longer residence time, which will improve the hydrogen production performance [41]. Obviously, the phenomenon was consistent with most of the results shown in Fig. 6. From this point of view, it could be tentatively conclude that if the middle portion porosity of a PCFSF-SLR were higher, generally the flow velocity distribution of the catalyst support would be more uniform. The third phenomenon was that when the middle portion porosity of a PCFSF-SLR was 0.9, the difference of the average velocity magnitude between the inlet manifold and the outlet manifold was the smallest, while when the middle portion porosity was 0.8, the difference was the largest. It would not be difficult to infer that lower difference of the velocity magnitude between the inlet manifold and the outlet manifold of a PCFSF-SLR would result into more uniform velocity distribution in the catalyst support. The fourth observation was that for two PCFSF-SLRs with the same middle portion porosity (e.g. 0.7-0.9-0.8 and 0.8-0.9-0.7), the flow velocity distributions seemed rotationally symmetrical to each other, especially for the input and output manifolds. This was attributed to the reactant feed direction [54]. As it could be seen, for two PCFSF-SLRs with the same middle portion porosity, different reactant feed direction would lead to different average velocity magnitude in the same porosity portion and in the whole PCFSF-SLR.

Combining with the last three phenomena, the data shown in Fig. 6 could be fully explained. For example, the average velocity magnitude of the whole PCFSF-SLR of 0.7-0.9-0.8, as well as the difference of the average velocity magnitude between the inlet manifold and the outlet manifold, was the smallest, indicating that the flow velocity distribution was more uniform. This was consistent with the fact that the hydrogen production performance of PCFSF-SLR of 0.7-0.9-0.8 was the best. However, although the average velocity magnitude of the whole PCFSF-SLR of 0.9-0.8-0.7 was smaller than that of the whole PCFSF-SLR of 0.7-0.8-0.9, the difference of the average velocity magnitude between the inlet manifold and the outlet manifold was the largest. This weakened and even overwhelmed the positive effect of the lower average velocity magnitude of a whole PCFSF-SLR, and making the hydrogen production performance of the two PCFSF-SLRs closer to each other and even flipped.

Hydrogen selectivity and CO concentration

Fig. 8(a) and (b) demonstrated the hydrogen selectivity and CO concentration of PCFSF-SLRs under different temperatures (from 280 °C to 380 °C) and fixed GHSV (16,252.4 ml/(g·h)). It was found that the hydrogen selectivity for PCFSF-SLRs of 0.7-0.9-0.8 and 0.8-0.9-0.7 was higher and could maintain over 82%, and that the CO concentration for PCFSF-SLRs of 0.7-0.9-0.8, 0.8-0.9-0.7 and 0.9-0.8-0.7 was less than 2.1%. In addition, as temperature rose, the overall hydrogen selectivity of all PCFSF-SLRs did not change significantly, while the CO concentration increased. In general, an increase in temperature increased the methanol conversion and therefore the hydrogen selectivity. However, the temperature rise also suppressed the WGS reaction (Eq. (4)), thus causing an increase in CO concentration [47].

Fig. 8(c) and (d) presented the hydrogen selectivity and CO concentration of PCFSF-SLRs under different GHSVs with the temperature fixed as 300 °C. It was found that the hydrogen selectivity for PCFSF-SLRs of 0.7-0.9-0.8 and 0.8-0.9-0.7 was maintained above 84%, and the CO concentration for PCFSF-SLRs of 0.7-0.9-0.8, 0.8-0.9-0.7 and 0.9-0.8-0.7 was less than 1.3%. Moreover, there was no significant change in the overall hydrogen selectivity and CO concentration. Generally, an

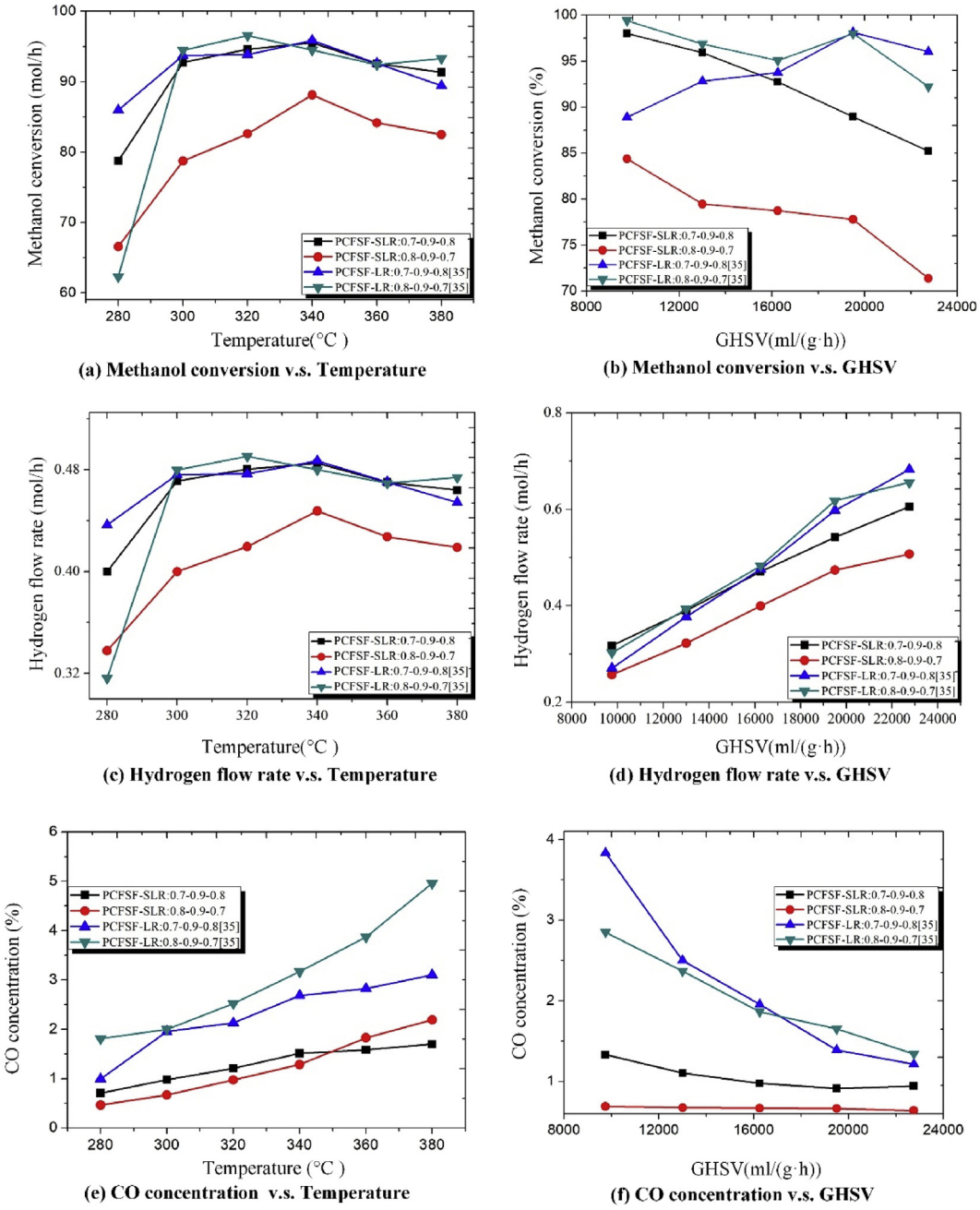

Fig. 9 – Comparison of methanol conversion and CO concentration for different PCFSFs under different reaction temperatures and GHSVs.

increase in GHSV would result in shorter residence time of the reactants in catalyst supports, thus reducing the overall reaction efficiency. However, the activation energy between different reactions was mainly affected by temperature, so when the temperature was constant, the efficiency of different reactions decreased in the same proportion. Consequently, the proportion of hydrogen and CO in the product was also relatively constant as shown in Fig. 8(c) and (d).

More importantly, it would not be difficult to found that the reaction performance shown in Fig. 8 was highly consistent with that in Fig. 6. For example, it was found that PCFSF-SLRs of 0.7-0.9-0.8 and 0.8-0.9-0.7 had higher hydrogen selectivity and lower CO concentration, while the PCFSF-SLR of 0.8-0.7-0.9 had the highest CO concentration. The explanations were similar to that discussed in Fig. 7, thus would not be gone into.

Comparison of reaction characteristics for PCFSF-SLRs and PCFSF-LRs

Similar to PCFSF-LRs studied in [40], PCFSF-SLRs of 0.7-0.9-0.8 and 0.8-0.9-0.7 showed relatively better reaction performance. Fig. 9 presented the methanol conversion, hydrogen flow rate and CO concentration of PCFSF-LRs and PCFSF-SLRs with better performance under different reaction temperatures and GHSVs. It could be found from Fig. 9(a) that the two kinds of PCFSFs had a similar trend of methanol conversion with temperature, and the methanol conversion of PCFSF-SLR of 0.7-0.9-0.8 was almost the same with that of PCFSF-LRs of 0.7-0.9-0.8 and 0.8-0.9-0.7. This was also nearly the same for methanol conversion with GHSV for the two kinds of PCFSFs as shown in Fig. 9(b). Exceptions were that, the methanol conversion of PCFSF-LRs was less affected by GHSV and remained on a higher level, while the methanol conversion of PCFSF-SLRs decreased with the increase of GHSV. Since hydrogen flow rate is closely related to methanol conversion, the relationships between the hydrogen flow rates of the two kinds of PCFSFs shown in Fig. 9(c) and Fig. 9(d) were also similar to that between the methanol conversions shown in Fig. 9(a) and Fig. 9(b). However, from Fig. 9(e) and Fig. 9(f) it could be observed that the CO concentration of PCFSF-SLRs with temperature and GHSV was obviously lower than that of PCFSF-LRs. This meant that the two PCFSF-SLRs were better than the corresponding PCFSF-LRs in reducing CO concentration.

The difference of the hydrogen production performance between the two kinds of PCFSFs could also be tentatively explained based on the flow velocity distributions. As observed from Fig. 10 and Fig. 7, the most obvious difference of the flow velocity distributions between the two kinds of PCFSFs was the way the reactants passed through the catalyst supports. For PCFSF-SLRs, the reactants would not flow from one porosity portion to another. This made the velocity distribution of each porosity portion relatively independent. Whereas, for PCFSF-LRs, it was obvious that the reactants would flow from one porosity portion to another (see the porosity portion configuration of PCFSF-LRs shown in Fig. 1(b) and the flow velocity distributions shown in Fig. 10). This would make the reactants distributed in the PCFSF-LRs more uniformly. In addition, it could be found from Figs. 10 and 1(b) that PCFSF-LRs with middle

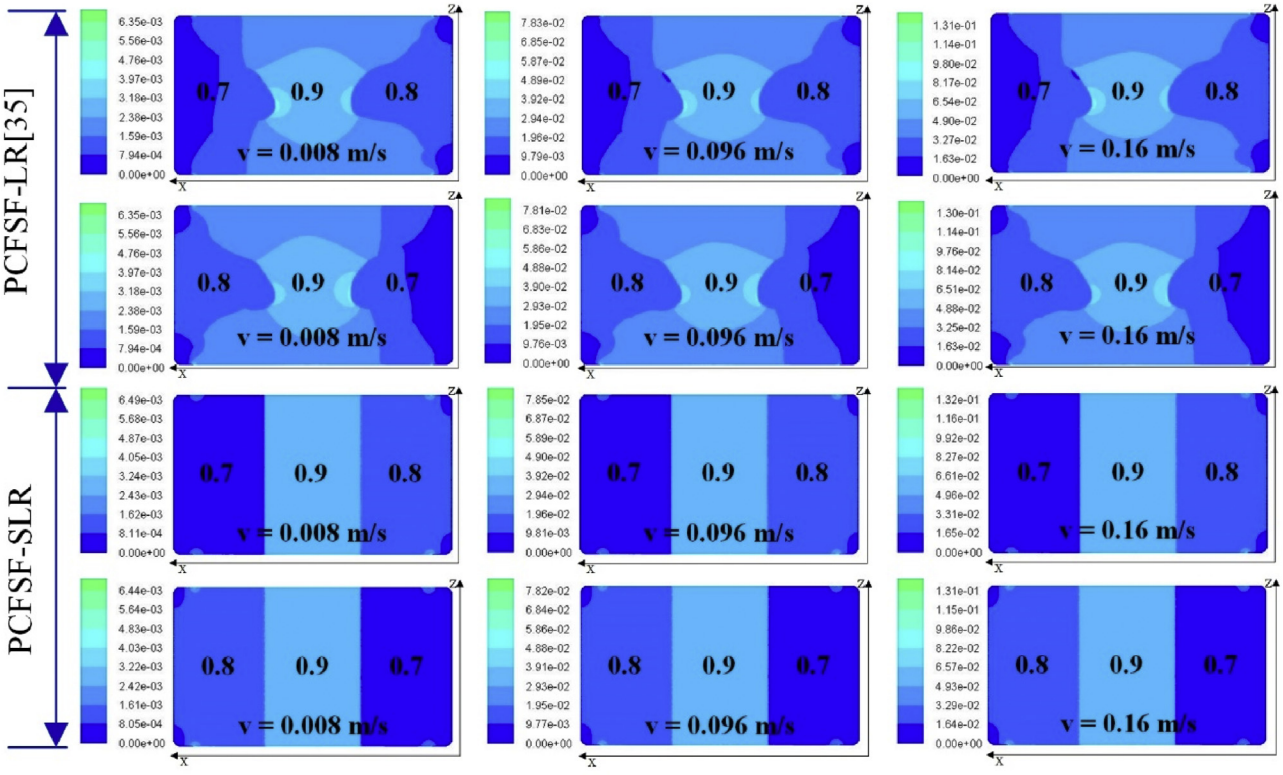

Fig. 10 – Flow distributions of different PCFSFs with middle porosity of 0.9 under different inlet velocity v.

porosity of 0.9 could make the flow velocity distribution near the inlet and outlet more uniform than that of the corresponding PCFSF-SLRs. More importantly, the middle portion with porosity of 0.9 in PCFSF-LRs enlarged the high-velocity area, making the flow velocity magnitude decreased from the center to the side more smoothly, which was a positive factor to enhance the reaction performance [54]. All these factors together made the methanol conversion of the PCFSF-LRs of 0.7-0.9-0.8 and 0.8-0.9-0.7 kept on a relatively higher level. However, when leaving a PCFSF-LR, most of the reactants and products would firstly flow from the side portions to the middle portion and then flow from the middle portion into the outlet manifold. This was different with PCFSF-SLRs and increased the probability of trapping the reactants and products in PCFSF-LRs. As a result, the WGS reaction (Eq. (3)) would be further suppressed, making the CO concentration of PCFSF-LRs relatively higher than that of PCFSF-SLRs. This in turn benefited the methanol conversion of the two PCFSF-SLRs, and even making the methanol conversion of the PCFSF-SLR of 0.7-0.9-0.8 close to that of the two PCFSF-LRs.

Based on the above analyses, it could be tentatively conclude that the proposed PCFSF-SLRs could improve the manufacturability of the velocity distribution-based gradient PCFSF, and at the same time maintain the performance of hydrogen production as closely as possible to the gradient PCFSF with curved interfaces, thus warranting the feasibility of the simplified catalyst support.

Conclusions

In order to improve the manufacturability of gradient PCFSFs with curved porosity portion interfaces, this paper developed a new and simplified gradient PCFSF with planar porosity portion interfaces, termed as PCFSF-SLRs. The reaction characteristics of PCFSF-SLRs loaded with Cu/Zn/Al/Zr catalyst for MSR were investigated under different reaction temperatures and GHSVs. Results indicated that the reaction characteristics of PCFSF-SLRs were similar to those of the previously developed PCFSF-LRs with curved porosity portion interfaces [40]. More importantly, the carbon monoxide concentration of PCFSF-SLR of 0.7-0.9-0.8 was better than that of the best PCFSF-LRs. The results demonstrated that it was feasible to simplify the curved porosity portion interfaces of PCFSF-LRs without dramatic decrease of hydrogen production performance. Hence, the proposed PCFSF-SLR with better manufacturability is a superior alternative to gradient PCFSFs with curved porosity portion interfaces. However, although the performance of PCFSF-SLRs, as well as the comparisons of PCFSF-SLRs and PCFSF-LRs, was analyzed to some extent from the perspective of flow velocity distribution, the underlying mechanisms attributed to the reaction characteristics of PCFSF-SLRs and the difference between the two kinds of PCFSFs were still yet to be revealed. This will be investigated by combining numerical and experimental studies in our future work, to design gradient PCFSFs more reasonably.

Acknowledgement

This work is financially supported by the Nature Science Foundation of China (51575192, 51775192 and 51875210), the Science & Technology Research Program of Guangdong (2016A030310409 and 2018B030311032), Joint Funds of the National Natural Science Foundation of China and Guangdong (U1601203), the Science & Technology Program of Guangzhou, China (201804010420), the Opening Project of Key Laboratory of Polymer Processing Engineering (South China University of Technology), Ministry of Education, and the Fundamental Research Funds for the Central Universities (2017MS019).

REFERENCES

[1] Colpan CO, Dincer I, Hamdullahpur F. A review on macro-level modeling of planar solid oxide fuel cells. Int J Energy Res 2010;32:336–55.
[2] Jia J, Abudula A, Wei L, Yue S. Performance comparison of three solid oxide fuel cell power systems. Int J Energy Res 2014;37:1821–30.
[3] Ni M, Leung MKH, Leung DYC. Ammonia-fed solid oxide fuel cells for power generation—a review. Int J Energy Res 2010;33:943–59.
[4] Xie J, Hao W, Wang F. The analysis of interfacial thermal stresses of solid oxide fuel cell applied for submarine power. Int J Energy Res 2018;42:2010–20.
[5] Lutz AE, Larson RS, Keller JO. Thermodynamic comparison of fuel cells to the Carnot cycle. Int J Hydrogen Energy 2002;27:1103–11.
[6] Akkaya AV. Electrochemical model for performance analysis of a tubular SOFC. Int J Energy Res 2010;31:79–98.
[7] Dong JS, Yoon WL, Yoon YG, Park SH, Park GG, Kim CS. Development of a micro fuel processor for PEMFCs. Electrochim Acta 2004;50:719–23.
[8] Chandan A, Hattenberger M, El-Kharouf A, Du S, Dhir A, Self V, et al. High temperature (HT) polymer electrolyte membrane fuel cells (PEMFC) – a review. J Power Sources 2013;231:264–78.
[9] Peighambardoust SJ, Rowshanzamir S, Amjadi M. Review of the proton exchange membranes for fuel cell applications. Int J Hydrogen Energy 2010;35:9349–84.
[10] Patil AS, Dubois TG, Sifer N, Bostic E, Gardner K, Quah M, et al. Portable fuel cell systems for America's army: technology transition to the field. J Power Sources 2004;136:220–5.
[11] Shuirong L, Jinlong G. Strategies for improving the performance and stability of Ni-based catalysts for reforming reactions. ChemInform 2015;46:7245–56.
[12] Wang T, Ma H, Zeng L, Li D, Tian H, Xiao S, et al. Highly loaded Ni-based catalysts for low temperature ethanol steam reforming. Nanoscale 2016;8:10177–87.
[13] Li D, Li X, Gong J. Catalytic reforming of oxygenates: state of the art and future prospects. Chem Rev 2016;116:11529–653.
[14] Liu Q, Hong H, Yuan J, Jin H, Cai R. Experimental investigation of hydrogen production integrated methanol steam reforming with middle-temperature solar thermal energy. Appl Energy 2009;86:155–62.
[15] Wang G, Wang F, Li L, Zhang G. Experiment of catalyst activity distribution effect on methanol steam reforming performance in the packed bed plate-type reactor. Energy 2013;51:267–72.
[16] Kiwi-Minsker L, Renken A. Microstructured reactors for catalytic reactions. ChemInform 2006;110:2–14.

[17] Aartun I, Silberova B, Venvik H, Pfeifer P, Görke O, Schubert K, et al. Hydrogen production from propane in Rh-impregnated metallic microchannel reactors and alumina foams. Catal Today 2005;105:469–78.
[18] Montebelli A, Visconti CG, Groppi G, Tronconi E, Cristiani C, Ferreira C, et al. Methods for the catalytic activation of metallic structured substrates. Catal Sci Technol 2014;4:2846–70.
[19] Zhou W, Tang Y, Wan ZP, Long-Sheng LU, Yong C, Pan MQ. Preparation of oriented linear copper fiber sintered felt and its performance. Trans Nonferrous Metals Soc China 2007;17:1028–33.
[20] Wießmeier G, Schubert K, Hönicke D. Monolithic microreactors possessing regular mesopore systems for the successful performance of heterogeneously catalysed reactions. Berlin, Heidelberg: Springer Berlin Heidelberg; 1998. p. 20–6.
[21] Granlund MZ, Görke O, Pfeifer P, Pettersson LJ. Comparison between a micro reactor with multiple air inlets and a monolith reactor for oxidative steam reforming of diesel. Int J Hydrogen Energy 2014;39:18037–45.
[22] Huang YX, Jang JY, Cheng CH. Fractal channel design in a micro methanol steam reformer. Int J Hydrogen Energy 2014;39:1998–2007.
[23] Mei D, Liang L, Qian M, Lou X. Modeling and analysis of flow distribution in an A-type microchannel reactor. Int J Hydrogen Energy 2013;38:15488–99.
[24] Pan M, Feng Z, Jiang L. Reaction characteristics of methanol steam reforming inside mesh microchannel reactor. Int J Hydrogen Energy 2016;41:1441–52.
[25] Zhou W, Deng W, Lu L, Zhang J, Qin L, Ma S, et al. Laser micro-milling of microchannel on copper sheet as catalyst support used in microreactor for hydrogen production. Int J Hydrogen Energy 2014;39:4884–94.
[26] Zhou W, Ke Y, Wang Q, Wan S, Lin J, Zhang J, et al. Development of cylindrical laminated methanol steam reforming microreactor with cascading metal foams as catalyst support. Fuel 2017;191:46–53.
[27] Yu H, Chen H, Pan M, Tang Y, Zeng K, Feng P, et al. Effect of the metal foam materials on the performance of methanol steam micro-reformer for fuel cells. Appl Catal A Gen 2007;327:106–13.
[28] Tang Y, Zhou W, Pan M, Chen H, Liu W, Hao Y. Porous copper fiber sintered felts: an innovative catalyst support of methanol steam reformer for hydrogen production. Int J Hydrogen Energy 2008;33:2950–6.
[29] Koga Hirotaka, Kitaoka Takuya, Nakamura Mitsuyoshi, et al. Influence of a fiber-network microstructure of paper-structured catalyst on methanol reforming behavior. J Mater Sci 2009;44:5836–41.
[30] Pan M, Zhong Y. Analysis of key factors influencing the evaporation performances of an oriented linear cutting copper fiber sintered felt. Heat Mass Transf 2017;54:1–8.
[31] Xu ZJ, Wang QH, Yang S, Li JR. Active multi-scale modeling and gas permeability study of porous metal fiber sintered felt for proton exchange membrane fuel cells. Int J Hydrogen Energy 2016;41:7393–407.
[32] Dalwadi MP, Griffiths IM, Bruna M. Understanding how porosity gradients can make a better filter using homogenization theory. In: Proceedings of the royal society a mathematical physical & engineering sciences; 2015. p. 471.
[33] Chun JH, Jo DH, Kim SG, Park SH, Lee CH, Lee ES, et al. Development of a porosity-graded micro porous layer using thermal expandable graphite for proton exchange membrane fuel cells. Renew Energy 2013;58:28–33.
[34] Hor JL, Jiang Y, Ring DJ, Riggleman RA, Turner KT, Lee D. Nanoporous polymer-infiltrated nanoparticle films with uniform or graded porosity via undersaturated capillary rise infiltration. ACS Nano 2017;11:3229.
[35] Zeschky J, Höfner T, Arnold C, Weißmann R, Bahloul-Hourlier D, Scheffler M, et al. Polysilsesquioxane derived ceramic foams with gradient porosity. Acta Mater 2005;53:927–37.
[36] Lv B, Fan X, Li D, Wang TJ. Towards enhanced sintering resistance: air-plasma-sprayed thermal barrier coating system with porosity gradient. J Eur Ceram Soc 2017;38.
[37] Hamedani HA, Baniassadi M, Sheidaei A, Pourboghrat F, Rémond Y, Khaleel M, et al. Three-dimensional reconstruction and microstructure modeling of porosity-graded cathode using focused ion beam and homogenization techniques. Fuel Cells 2014;14:91–5.
[38] Zhang Y, Verma A, Pitchumani R. Optimum design of polymer electrolyte membrane fuel cell with graded porosity gas diffusion layer. Int J Hydrogen Energy 2016;41:8412–26.
[39] Zhou W, Wang Q, Li J, Tang Y, Huang Z, Zhang J, et al. Hydrogen production from methanol steam reforming using porous copper fiber sintered felt with gradient porosity. Int J Hydrogen Energy 2015;40:244–55.
[40] Wang QH, Yang S, Zhou W, Li JR, Xu ZJ, Ke YZ, et al. Optimizing the porosity configuration of porous copper fiber sintered felt for methanol steam reforming micro-reactor based on flow distribution. Appl Energy 2018;216:243–61.
[41] Zhou W, Tang Y, Pan M, Wei X, Chen H, Xiang J. A performance study of methanol steam reforming microreactor with porous copper fiber sintered felt as catalyst support for fuel cells. Int J Hydrogen Energy 2009;34:9745–53.
[42] Zhou W, Tang Y, Wang QH, Hui KS, Hui KN, Wan ZP, et al. Optimization of catalyst loading for porous copper fiber sintered felts used in methanol steam reforming microreactors. Chem Eng Technol 2013;36:307–14.
[43] Yong ST, Ooi CW, Chai SP, Wu XS. Review of methanol reforming-Cu-based catalysts, surface reaction mechanisms, and reaction schemes. Int J Hydrogen Energy 2013;38:9541–52.
[44] Sá S, Silva H, Brandão L, Sousa JM, Mendes A. Catalysts for methanol steam reforming—a review. Appl Catal B Environ 2010;99:43–57.
[45] Li YF, Dong XF, Lin WM. Effects of ZrO-promoter on catalytic performance of CuZnAlO catalysts for production of hydrogen by steam reforming of methanol. Int J Hydrogen Energy 2004;29:1617–21.
[46] Breen JP, Ross JRH. Methanol reforming for fuel-cell applications: development of zirconia-containing Cu–Zn–Al catalysts. Catal Today 1999;51:521–33.
[47] Wang G, Feng W, Li L, Zhang G. Experimental investigation of axially non-uniform catalysis for methanol steam reforming. J Power Sources 2014;250:306–12.
[48] Qian M, Mei D, Yao Z, Liu B, Lou X, Chen Z. Flow manifold optimization for a uniform velocity distribution in a laminated microreactor with micro-pin-fin arrays. Chem Eng Technol 2014;37:1112–20.
[49] Mohammadi M, Jovanovic GN, Sharp KV. Numerical study of flow uniformity and pressure characteristics within a microchannel array with triangular manifolds. Comput Chem Eng 2013;52:134–44.
[50] Pistoresi C, Fan Y, Luo L. Numerical study on the improvement of flow distribution uniformity among parallel mini-channels. Chemical Engineering & Processing Process Intensification 2015;95:63–71.
[51] Pan M, Wei XL, Zeng D, Tang Y. Trend prediction in velocity distribution among microchannels based on the analysis of frictional resistances. Chem Eng J 2010;164:238–45.

[52] Liu H, Li P. Even distribution/dividing of single-phase fluids by symmetric bifurcation of flow channels. Int J Heat Fluid Flow 2013;40:165–79.
[53] Pan M, Li L, Shao X, Zeng D. Velocity distribution inside a laminated-sheet microchannel reactor. Chem Eng Technol 2015;38:336–44.
[54] Xu ZJ, Yang S, Hu GH, Wang QH, Li JR. Numerical study of flow distribution uniformity for the optimization of gradient porosity configuration of porous copper fiber sintered felt for hydrogen production through methanol steam reforming micro-reactor. Int J Hydrogen Energy 2018;43:4335–70.